PHYSICAL REVIEW B VOLUME 38, NUMBER 15 15 NOVEMBER 1988-II

Noble-gas ion bombardment on clean silicon surfaces

A. H. M. Holtslag and A. van Silfhout
Department of Applied Physics, Twente University of Technology, P.O. Box 217, 7500AE Enschede, The Netherlands
(Received 10 March 1988)

Under UHV conditions clean *c*-Si(111) surfaces have been bombarded at room temperature by noble gases (He,Ne,Ar,Kr). Using spectroscopic ellipsometry, the implantation processes were continuously recorded. A low-dose behavior (amorphization) and a high-dose behavior (dilution) are observed. After termination of the bombardment, a self-anneal behavior appears and some experiments are discussed in order to explain the observed phenomena. After applying a monotonous temperature increase up to 1100 K, the noble gas desorbs and the surface layer returns to the original state, as can be seen from a closed trajectory in the $(\delta\psi,\delta\Delta)$ plane. The low-dose behavior is analyzed in the scope of a simple ellipsometric first-order approximation, and the results obtained are compared with theory. The dilution arising during the high-dose behavior can be explained ellipsometrically by means of microscopic surface roughness, and some complementary measurements are reported to verify this explanation.

I. INTRODUCTION

During ion bombardment on, or sputtering of, clean *c*-Si the various effects induced at the surface (surface roughness, surface-state changes, surface-anisotropy changes) and in the implanted layer (damage, implanted ions, dilatation, bubble formation, blistering) are reflected in changes of the complex dielectric function $\tilde{\epsilon}=\epsilon_1-i\epsilon_2$ and in the measurable ellipsometric quantities ψ and Δ $(\rho=\tan\psi e^{i\Delta})$. In previous publications methods to analyze those effects are pointed out in detail.[1,2] To get an idea of these effects induced at Ar^+-ion bombardments (normal incidence, 2.2. keV) an example as shown in Fig. 1(a) will be discussed at first. In the $(\delta\psi,\delta\Delta)$ plane at three different wavelengths the measured ellipsometric quantities are shown during bombardment, and those bombardments are followed by desorption studies. Because the effects induced disappear due to the slow temperature increase ($\sim 7\times10^{-2}$ K/s) up to 1050 K closed trajectories are observed. In all cases the initial (ψ,Δ) values of clean *c*-Si as a function of temperature are taken as a reference. The trajectories $1\rightarrow2\rightarrow3$ and $1\rightarrow2\rightarrow3\rightarrow3'$ correspond to continuous bombardments at room temperature. The first trajectory is called the low-dose behavior because the large changes are induced due to low doses N_b (typical $N_b<0.1$ Å^{-2}). Trajectory $3\rightarrow3'$ is called the high-dose behavior: finally the ellipsometric values saturate at doses of $N_b\sim5$ Å^{-2}. At point 3 (3′) bombardments are turned off and at room temperature the change $3\rightarrow4$ $(3'\rightarrow4')$ is observed. This is called the self-anneal behavior, to be discussed in Sec. VII. The trajectories $4\rightarrow5\rightarrow6\rightarrow7$ and $4'\rightarrow5'\rightarrow6'\rightarrow7'$ correspond to the desorption of the noble gas due to the applied temperature increase up to 1050 K. The desorption experiments are discussed in previous papers.[1,3] A typical observation during the high-dose behavior is shown in Fig. 1(b) for Ne^+-, Ar^+-, and Kr^+-ion bombardments (2.2 keV). After the low-dose behavior the final changes in the $\delta\Delta$ are proportional and can be expressed as

$$\delta\Delta(\lambda_k)=a_{kl}+b_{kl}\delta\Delta(\lambda_l)\ , \tag{1}$$

even in such a way that $b_{kl}\sim1$. So the low-dose behavior can be seen as the change starting at (0,0) up to the line with a slope equal to b_{kl}. The high-dose behavior is directed along the line with slope b_{kl}. This behavior will be pointed out in Sec. II D.

In order to explain the observed low-dose behavior, use will be made of the expressions of Kinchin and Pease,[4] Morehead and Crowder,[5] and Thompson, Walker, and Davies.[6(a),6(c)]

In the low-energy region Kinchin and Pease show that the number of target atoms displaced by a primary coil (nuclear energy E) should be $E/2E_d$ where E_d denotes the displacement energy of a target atom on the order of 15 eV for silicon. This well-known formula has often been reexamined in the literature. Nowadays the value $0.41E/E_d$ is more often used. A model for the formation of amorphous silicon by ion bombardment is given by Morehead and Crowder. In this model the penetrating incident atom first creates a highly disordered region where many bonds are broken and atoms are displaced. These displaced atoms form new bonds and change their positions to form a stable amorphous phase during a time τ, on the order of 10^{-9} s. The final region is arbitrarily represented by a cylinder with a length equal to the range r of the incident atom and with a surface A_a equal to

$$(A_a)^{1/2}=\frac{(S_n)^{1/2}-K'e^{-E_a/kT}}{(\bar{E}n_{\rm Si})^{1/2}}\ ,$$
$$K'=2\left[\frac{\tau a^2\nu\bar{E}n_{\rm Si}}{6}\right]^{1/2}. \tag{2}$$

In this formula S_n is considered as an energy-independent nuclear energy loss, $\bar{E}$ an effective displacement energy, $n_{\rm Si}$ the density of a silicon target (0.05 Å^{-3}), and K' an

 ©1988 The American Physical Society

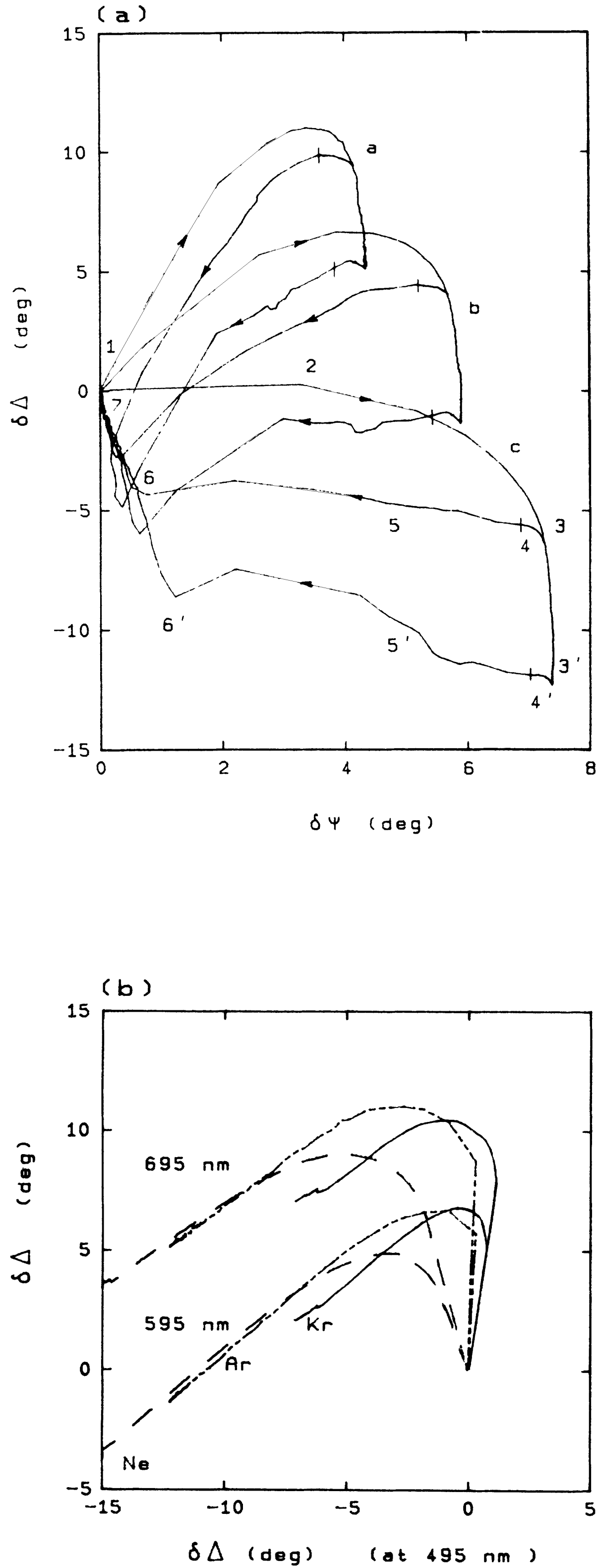

FIG. 1. (a) The ellipsometric results during ion bombardment, self-anneal behavior, and desorption experiments of Ar^+ in the ($\delta\psi,\delta\Delta$) plane, at (a) 695 nm, (b) 595 nm, and (c) 495 nm. The numbers are explained in the text. (b) An illustration of the linear relation between the $\delta\Delta$ values as given in (a) during the high-dose behavior. Included are the Ne^+-, Ar^+-, and Kr^+-bombardment results ($\phi_0=70.25°$).

abbreviation of the property reflecting the diffusion of vacancies during the time τ with rate constant ν and activation energy E_a. Fitting the available experimental data they obtain $E_a=60$ meV and $K'=36.4$ (eV/Å)$^{1/2}$. The amount of displaced atoms $\eta_d=rA_a n_{\text{Si}}$ and becomes for $S_n=E/r$ equal to $E/\bar{E}$ at zero temperature. So, in fact, they also use the formula of Kinchin and Pease, however taking into account the escape of vacancies by thermal diffusion during the time τ.

Thompson, Walker, and Davies[6(c)] observed an empirical relation at a temperature of 35 K for the number of displaced atoms in c-Si, irradiated with a variety of ions. They used energies higher than 15 keV and give the relation

$$\eta_d^{35}=251M_p^{0.75}\left[1-\exp\left(-\frac{E_n}{30\text{ keV}}\right)\right]+0.032E_n \ . \quad (3)$$

In this formula M_p denotes the projectile mass in atomic mass units of the incident ion and E_n the energy lost in nuclear collisions expressed in keV. If this formula also holds for low energies $E_n \ll 30$ keV then the expression can be approximated by

$$\eta_d^{35}\sim 8.37M_p^{0.75}E_n \ .$$

It will be shown that the above-mentioned expressions can be successfully tested by means of ellipsometric measurements. After a general description of the ellipsometric response and a first-order approximation in Sec. II, the above-mentioned models will be used to describe the low-dose behaviors of sputtering experiments (45° angle of incidence) and ion bombardments (normal incidence) in Secs. III and IV, respectively.

In Sec. V some results of the high-dose behavior are described and Sec. VI gives some complementary measurements in order to verify the explanation of the observed dilution. In Sec. VII some experiments during the self-anneal behavior are discussed.

II. ELLIPSOMETRY

A. General

Spectroscopic ellipsometry is used to measure, as a function of the photon energy, the complex value $\tilde{\rho}$, the quotient of the parallel ($\tilde{r}_p$) and the perpendicular ($\tilde{r}_s$) reflection coefficients

$$\tilde{\rho}=\frac{\tilde{r}_p}{\tilde{r}_s}=\tan\psi\, e^{j\Delta}, \quad \tilde{r}_\nu=\tilde{E}_\nu^-/\tilde{E}_\nu^+ , \quad \nu=p,s \ . \quad (4)$$

Measurements are presented as (ψ,Δ) pairs or as ($\delta\psi,\delta\Delta$) pairs which refer to an initial condition.

For a three-phase system as shown in Fig. 2, the reflection coefficients become[7]

$$\tilde{r}_\nu=\frac{\tilde{r}_{\nu 0l}+\tilde{r}_{\nu lc}e^{-i\tilde{x}}}{1+\tilde{r}_{\nu 0l}\tilde{r}_{\nu lc}e^{-i\tilde{x}}}, \quad \nu=p,s \quad (5)$$

with

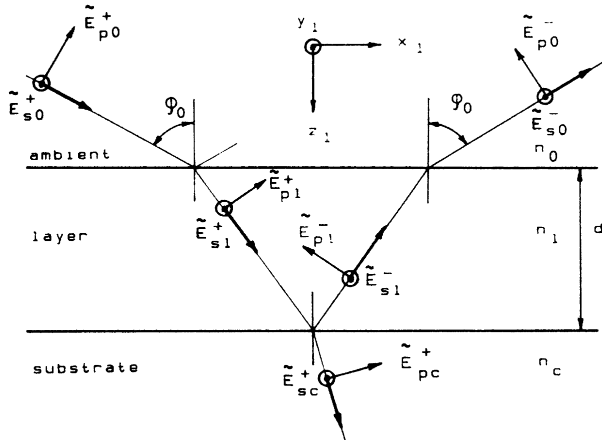

FIG. 2. The propagating electromagnetic plane waves in a three-phase system.

$$\tilde{x}=\frac{4\pi d}{\lambda_0}\left[\frac{\tilde{\epsilon}_l}{\epsilon_0}-\sin^2\phi_0\right]^{1/2} \tag{6}$$

and with Fresnel reflection coefficients given by ($jk=0l$ or lc)

$$\tilde{r}_{pjk}=\frac{\tilde{n}_k\cos\tilde{\phi}_j-\tilde{n}_j\cos\phi_k}{\tilde{n}_k\cos\tilde{\phi}_j+\tilde{n}_j\cos\phi_k}\ ,\quad \tilde{r}_{sjk}=\frac{\tilde{n}_j\cos\tilde{\phi}_j-\tilde{n}_k\cos\tilde{\phi}_k}{\tilde{n}_j\cos\tilde{\phi}_j+\tilde{n}_k\cos\tilde{\phi}_k} \tag{7}$$

and where Snell's law has to be obeyed:

$$n_0\sin\phi_0=\tilde{n}_l\sin\tilde{\phi}_l=\tilde{n}_c\sin\tilde{\phi}_c\ . \tag{8}$$

A matrix representation can be formulated for a multilayer system.[7] Alternatively, a recursive formula can be obtained by applying Eq. (5) again, if $\tilde{r}_{vlc}$ is replaced by the reflection coefficient of the underlying layers.

B. First-order approximation

If $|\tilde{x}|\ll 1$ which is illustrative, $\tilde{\rho}$ can be approximated to first order in $\tilde{x}$ for a three-phase system:

$$\tilde{\rho}=\tilde{\rho}_c\left[1+i\tilde{\gamma}_c d\frac{(\tilde{\epsilon}_l-\epsilon_0)(\tilde{\epsilon}_l-\tilde{\epsilon}_c)}{\tilde{\epsilon}_l}\right] \tag{9}$$

with

$$\tilde{\gamma}_c=\frac{4\pi(\epsilon_0)^{1/2}\cos\phi_0}{\lambda_0(\tilde{\epsilon}_c-\epsilon_0)(\cot^2\phi_0-\epsilon_0/\tilde{\epsilon}_c)},\quad \tilde{\rho}_c=\frac{\tilde{r}_{p0c}}{\tilde{r}_{s0c}}\ . \tag{10}$$

The values $\tilde{\gamma}_c$ and $\tilde{\rho}_c$ depend only on substrate values c. Defining $\delta\tilde{\rho}$ by $\tilde{\rho}-\tilde{\rho}_c$, Eq. (9) can be written as

$$\frac{\delta\tilde{\rho}}{\tilde{\rho}_c}=\frac{2\delta\psi}{\sin\psi_c}+i\delta\Delta=i\tilde{\gamma}_c d\frac{(\tilde{\epsilon}_l-\epsilon_0)(\tilde{\epsilon}_l-\tilde{\epsilon}_c)}{\tilde{\epsilon}_l}\ . \tag{11}$$

By using Eq. (11), the unknown $\tilde{\epsilon}_l$ can be expressed in the measured values $\delta\psi$, $\delta\Delta$, and in the substrate values. It will give two roots. The positive has to be taken and the discriminant can be approximated again. Alternatively, if $[(\tilde{\epsilon}_l-\epsilon_0)/\tilde{\epsilon}_l]\sim 1$, the following simple expression is obtained:

$$d(\tilde{\epsilon}_l-\tilde{\epsilon}_c)=\frac{1}{\tilde{\gamma}_c}\left[\delta\Delta-\frac{2i\delta\psi}{\sin\psi_c}\right]\ . \tag{12}$$

The condition $|\tilde{x}|\sim(4\pi d/\lambda_0)|\tilde{\epsilon}_l/\epsilon_0|^{1/2}\ll 1$ means that Eq. (12) only holds for thin layers. In such a case only the product $d(\tilde{\epsilon}_l-\tilde{\epsilon}_c)$ can be obtained.

As an example, this expression gives an idea of the effect of microscopic surface roughness on clean silicon substrates. Apply for instance a simple linear model on $\tilde{\epsilon}_l$, so $\tilde{\epsilon}_l-\tilde{\epsilon}_c=-\theta_v(\tilde{\epsilon}_c-\epsilon_0)$, and substitute this model as well as Eq. (10) in Eq. (12). It results in (substitute also $\epsilon_0/\tilde{\epsilon}_c\ll 1$)

$$\delta\Delta=-\frac{d\theta_v}{\lambda_0}4\pi(\epsilon_0)^{1/2}\cos\phi_0\tan^2\phi_0\ ,\qquad \delta\psi\approx 0\ \text{(first order)}\ . \tag{13}$$

For $\phi_0=70°$ and $d\theta_v=5$ Å at $\lambda_0=5000$ Å a value of $\delta\Delta=-1.86°$ is obtained.

C. A method of calculation to obtain the number of displaced atoms

In cases when only one process dominates a very simple calculation method is possible. Consider for instance the creation of an amorphous layer on top of a c-Si substrate due to sputtering or bombardment. As can be expected from the first-order approximation in Eq. (12), the values of $\delta\Delta$ and $\delta\psi$ will be proportional to the amount of amorphous clusters induced, because in the layer thickness d the dielectric constant changes from $\tilde{\epsilon}_c$ up to $\tilde{\epsilon}_l$. At low dose the changes will be small. Therefore it will be shown that for small values of $\delta\psi$ this value in the low-photon-energy range is equal to the integral

$$\delta\psi=\beta\int_0^d\theta_a(x)dx\ . \tag{14}$$

In this equation β is a function of wavelength, angle of incidence, and dielectric functions. This relationship will be used for the interpretation of sputter experiments carried out at low energies.

In Fig. 3(a) profiles $\theta_a(x)$ of amorphous silicon are shown as a function of depth x. These profiles do have in common that the integral in Eq. (14) is the same. The values $\delta\psi$ and $\delta\Delta$ can be calculated from the $\tilde{\epsilon}_a$ and $\tilde{\epsilon}_c$ values obtained previously[1,2] as a function of the parameter d for a wavelength of 495 nm. In Fig. 3(b) the exact results are shown if the dielectric constant $\tilde{\epsilon}_l$ of the layer is composed of a mixture of a-Si and c-Si and obeys a linear relation having the form

$$\tilde{\epsilon}_l=\theta_a\tilde{\epsilon}_a+\theta_c\tilde{\epsilon}_c,\quad \theta_c=1-\theta_a\ . \tag{15}$$

Indeed, both values $\delta\Delta$ and $\delta\psi$ are proportional with the total effective amorphous volume. However, the advantage of considering $\delta\psi$ is that in all cases investigated the same β is observed, in contrast to $\delta\Delta$. In this case the values of $\delta\psi$ are linear with the integral as given in Eq.

(14) up to $\delta\psi = 2.5°$. The value of β in this case is 0.102 deg/Å at 495 nm. Instead of a triangular profile, an equivalent rectangular one can be obtained with almost the same $\delta\Delta$. This equivalent rectangular profile has a base of $\frac{2}{3}d$ and an amorphous fraction $\theta_a = \frac{3}{4}$, see Fig. 3(a). In Fig. 3(c) the results are given if the dielectric constant obeys the effective-medium approximation (EMA) equation.[8] The conclusion still holds, however the initial slope in Fig. 3(c) now depends only a little on the shape of the profile. The value of β for the triangularly shaped profile is 0.10 deg/Å at 495 nm. (In the case of the triangularly shaped profile the calculation has been carried out for a 100-layer model.)

The above results indicate that for low values of $\delta\psi$, the influence of the shape of the profile is neglectable on $\delta\psi$. This simple calculation method has the advantage that a precise knowledge of $\tilde{\epsilon}_a$ and a model for $\tilde{\epsilon}_l$ are not necessary at all. Therefore it is a suitable tool for studying the total displaced number of atoms η_d at a low ion dose, because $\delta\psi$ will then be low. Also, $\delta\psi$ as a function

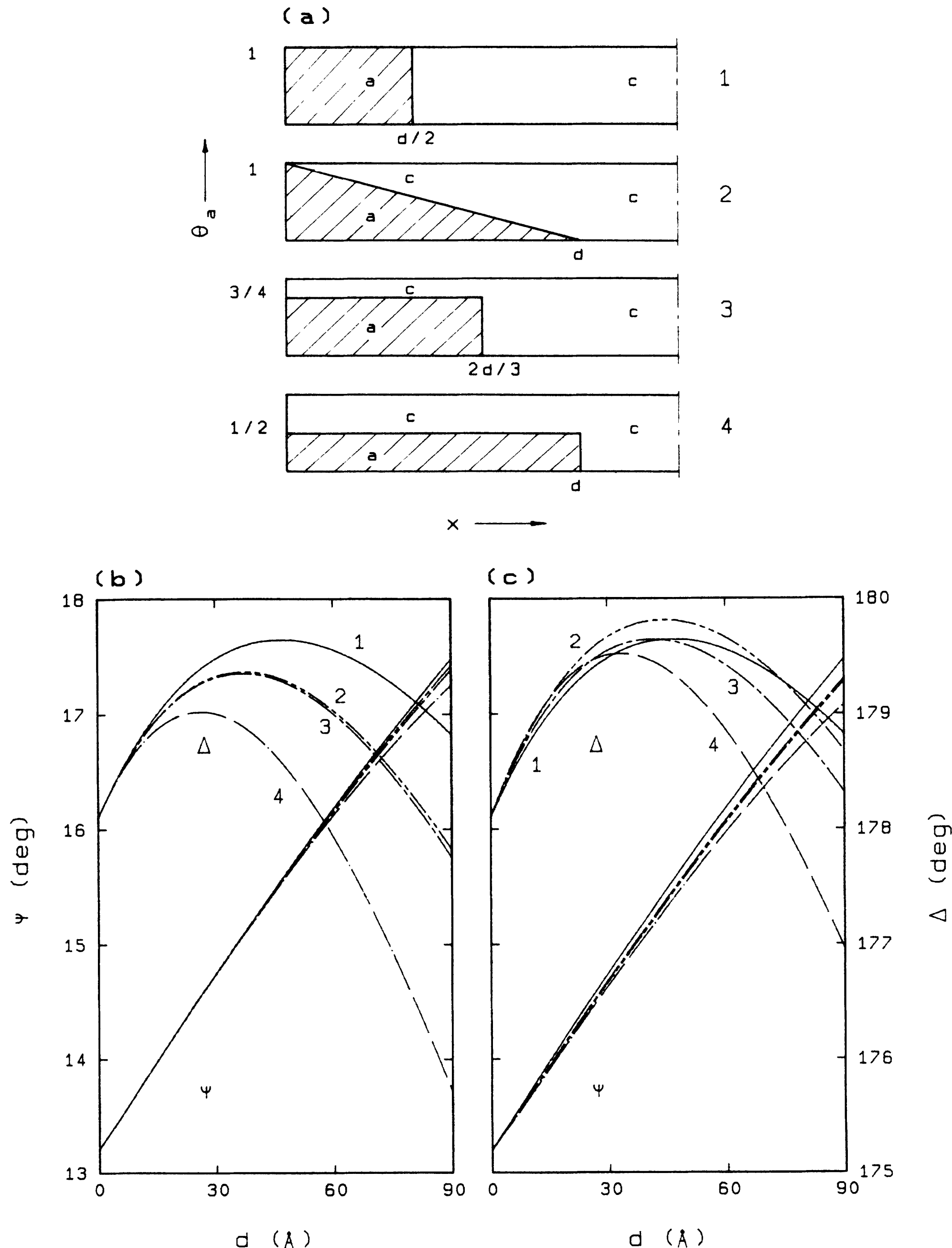

FIG. 3. (a) Profiles of $\theta_a(x)$ as a function of the depth x. In all cases the integral as given in Eq. (14) is the same. Also the position of the moment of inertia along the x axis of profiles 2 and 3 is the same, a denotes amorphous, c denotes crystalline. (b) and (c) The ellipsometric values $\delta\psi$ and $\delta\Delta$ of the profiles of (a) at increasing layer thickness d, calculated by assuming for $\tilde{\epsilon}_l$ (b) a linear and (c) an EMA equation, by making use of $\phi_0 = 70.25°$, $\lambda = 495$ nm, $\tilde{n}_c = 4.33 - i0.068$, and $\tilde{n}_a = 4.97 - i1.44$.

of time can be used to obtain the dynamical model, for instance to obtain the characteristic area A_a.

D. Surface roughness at the high-dose behavior

As a second example, we return to the large observed change in $\delta\Delta$ at the high-dose behavior, as shown in Fig. 1. This change is almost the same for all wavelengths at the low-photon-energy range. The corresponding change in $\delta\psi$, however, is much smaller than during the low-dose behavior, see Fig. 1(a).

The change in Δ due to microscopic surface roughness on c-Si is proportional to d/λ, see Eq. (13). Therefore, a coefficient $b_{kl}=\lambda_l/\lambda_k$ can be expected for surface roughness on c-Si. For surface roughness on a-Si a coefficient $b_{kl}\sim 1$ is observed. Therefore, a model calculation has been carried out, see Fig. 4(b), to explain the value b_{kl}. For some values of x_1 and d the change $\delta\Delta=\Delta_{sr}-\Delta_a$ is calculated as a function of the photon energy. The value Δ_a denotes the calculated Δ for an amorphous layer on top of c-Si with a layer thickness $d-\frac{1}{2}x_1$ and Δ_{sr} denotes the calculated value for the model in Fig. 4(a). The $\tilde{\epsilon}_a$ of the low-dose behavior is used for these calculations. The differences $\delta\Delta$ are not proportional to d/λ, but are almost horizontal lines as a function of the photon energy E. This explains a coefficient $b_{kl}\sim 1$.

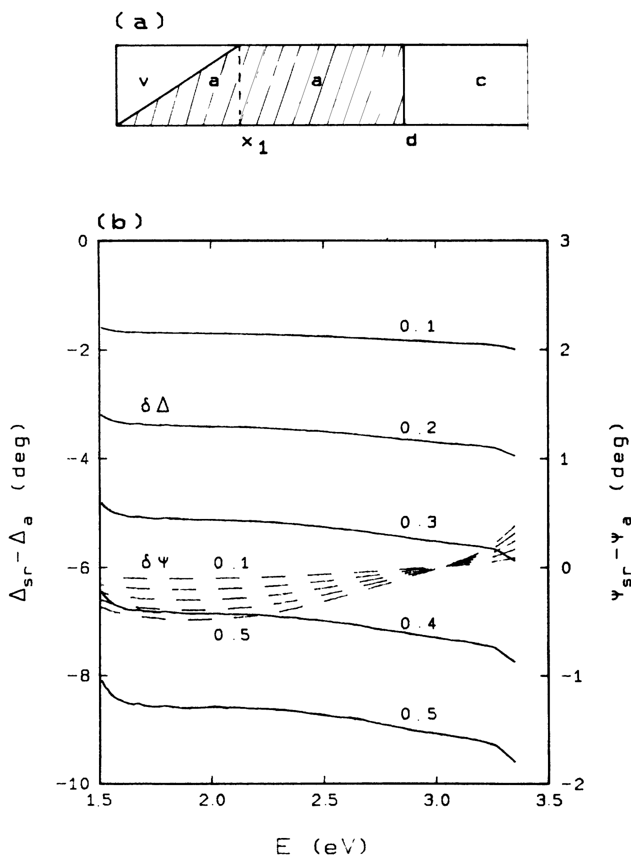

FIG. 4. (a) A schematic representation of the examined model, where v denotes voids, a denotes amorphous, and c denotes crystalline. (b) A model calculation to explain the linear relation between the $\delta\Delta$'s due to surface roughness. The parameters 0.1–0.5 correspond to the value $x_1/(d-x_1/2)$, see the model of (a), $d=100$ Å.

III. RESULTS OF SPUTTER EXPERIMENTS FOR He, Ne, Ar, AND Kr

The reported experiments are carried out in the UHV system as described in Ref. 9. In Figs. 5(a) and 5(b) the measured values of $\delta\psi$ and $\delta\Delta$ are shown as a function of the ion dose for He, Ne, Ar, and Kr sputter experiments on c-Si(111) samples at an acceleration voltage of 800 V, an ion flux 115 nA/cm^2, and an angle of incidence of the ions at 45°. The experimental results are also shown in the $(\delta\psi,\delta\Delta)$ plane of Fig. 5(c). The curves in the $(\delta\psi,\delta\Delta)$ plane do have the same envelope as the ion-bombardment curves. First some experimental remarks will be made before these results are discussed.

In contrast to the ion beam used for the bombardments it is difficult with our sputter gun to obtain a constant flux density over a large area. Therefore, the diameter of the light beam of the ellipsometer has been reduced to 1 mm, so that the light spot on the silicon surface is an ellipsoid with a short axis of 1 mm and a long axis of ≈ 3 mm. In this case the flux density is constant within 10%. Furthermore, the ion dose N_b is the incident ion dose on the sample without correction for reflection of ions at the silicon surface. Because the sputter gun is not equipped with a mass filter there will also be double-charged ions present in the ion beam. These double-charged ions will have a double energy with respect to the single-ionized ions and will have a higher ion range into the solid. The final observed layer thicknesses can therefore be affected by the ranges of higher-charged ions. The ions are created in the ionization chamber of the gun by impinging electrons of about 150 eV into the gas. As an estimated guideline for the production of double-ionized atoms with respect to the single charged, use can be made of the partial ionization cross section at 500 eV as given by Schram.[10] The production ratios can be obtained by dividing the partial ionization cross section of the two types of ions and will at least be less than 1% (He) up to 9% (Kr). Due to the presence of higher-ionized atoms it can take a long time before the $\delta\psi$ and $\delta\Delta$ values saturate.

In order to obtain the characteristic area A_a within the scope of the model of Morehead and Crowder,[5] the value of $\delta\psi$ should behave as an exponential function because, as shown in Sec. II C, $\delta\psi$ is proportional to the damage induced:

$$\delta\psi=\delta\hat{\psi}(1-e^{-A_aN_b})=\beta d(1-e^{-A_aN_b}) . \quad (16)$$

The exponential term $[1-\exp(-A_aN_b)]$ arises due to the overlap of the amorphous cylinders.[5,11] The maximum value denoted by $\delta\hat{\psi}$ corresponds to the final volume of the amorphous top layer while a value of $\beta=0.10$ deg/Å at 495 nm has to be used in the case of the EMA equation. The slope $\delta(\delta\psi)/\delta N_b$ can be written as

$$\frac{\delta(\delta\psi)}{\delta N_b}=\beta d A_a e^{-A_aN_b}=(\delta\hat{\psi}-\delta\psi)A_a \quad (17)$$

for the low-dose behavior, as long as the influence of the higher-ionized atoms can be neglected. The value of

$\delta(\delta\psi)/\delta N_b$ against $\delta\psi$ is shown in Fig. 6 for the recorded $\delta\psi$ values at 495 nm for the different noble gases. If Eq. (17) is valid we must observe in this figure straight lines for the low-dose behavior. First the part denoted by A in Fig. 6 will be disregarded. The intersection of the slope with the $\delta\psi$ axis at part C gives a final $\delta\hat{\psi}_c$ as reported in Table I. A layer thickness $d_c = \delta\hat{\psi}_c/\beta$ can be calculated from this value. This thickness corresponds to a calculated ion range, if we correct for an angle of incidence of 45°. By assuming that the observed layer thickness is of the order of $r\cos45°$, a good estimate of the observed layer thicknesses is obtained, see Table I. Therefore, the higher-ionized atoms do not affect the optical data in the measured ion-dose range very much.

Because part A of Fig. 6 cannot be described by Eq. (17), while part B seems to fulfill Eq. (17), the characteristic area A_a^B has first been calculated for part B to get an idea of that value. Furthermore, by extrapolating the slope at part B to the vertical axis, an impression of the production rate can be obtained. A_a^B and the initial production rate for part B, η_d^B, are given in Table I as well. These values are compared with the area $A_a^0 = S_n/\bar{E}n_{\mathrm{Si}}$ and the value η_d^{35} as predicted by Eq. (3). The data for $(A_a^B)^{1/2}$ and $(\bar{S}_n)^{1/2}$ are included in Fig. 9 and obey the same function as for the bombardments discussed in the next section.

Within the scope of the model of Morehead and Crowder, He^+ cannot make c-Si amorphous, because the

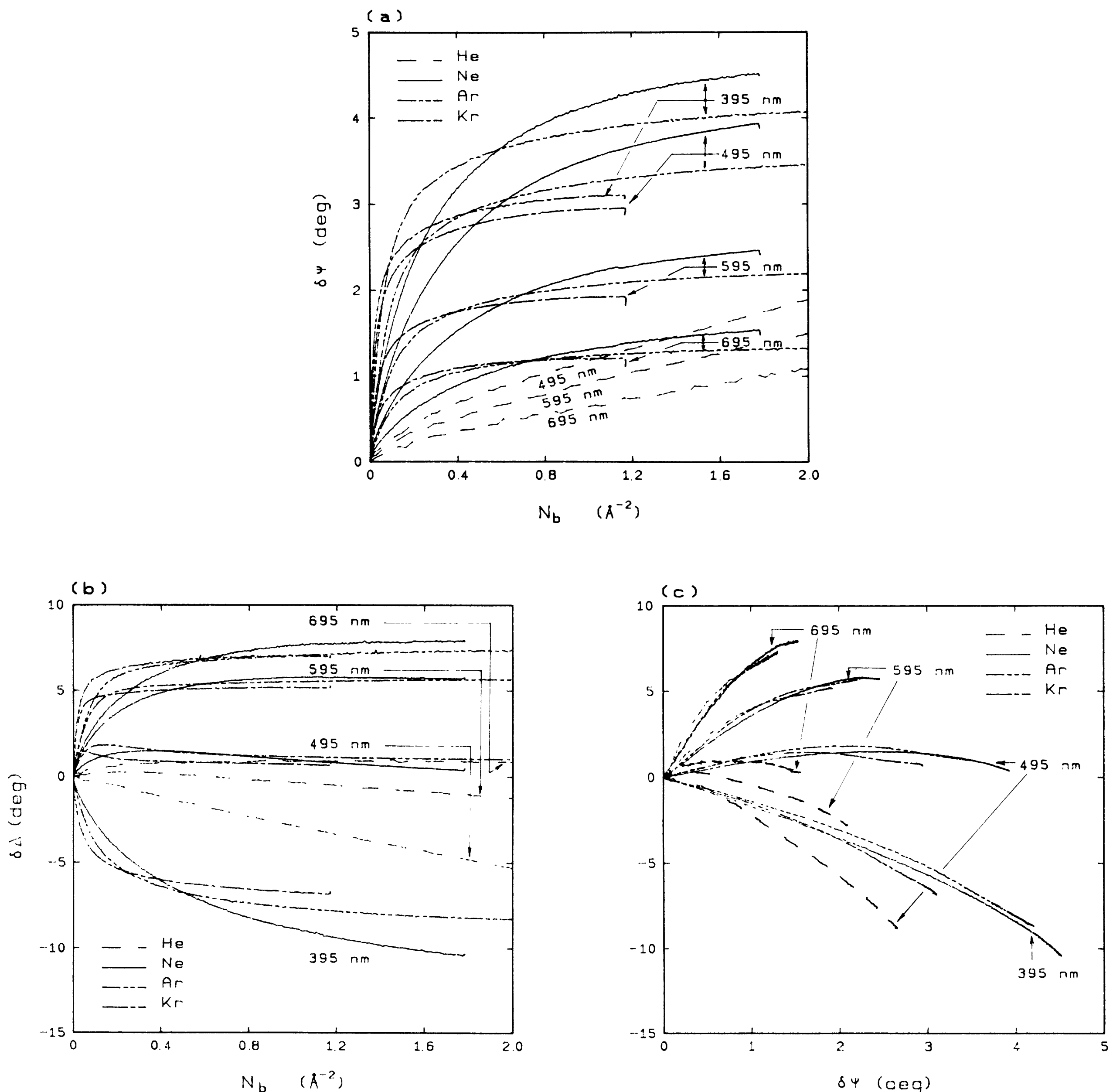

FIG. 5. (a) and (b) Results for He, Ne, Ar, and Kr sputter experiments at an acceleration voltage of 800 V, an ion flux of 115 nA/cm^2 and an angle of incidence of 45° ($\phi_0 = 70.25°$). (c) The results of (a) and (b) in the $(\delta\psi, \delta\Delta)$ plane.

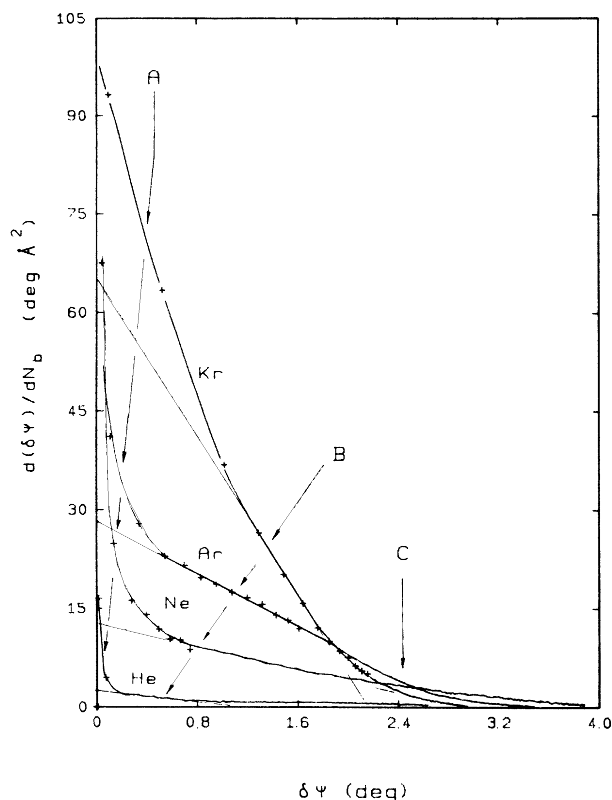

FIG. 6. The interpretation of the characteristic area A_a; see the text and Eq. (17) for an explanation.

square root of the area A_a^0 is smaller than 3.2 Å. However, there is a surprising result if part A of Fig. 6 is considered. By plotting $\log(\delta\psi)$ against $\log N_b$ we observe at a low dose a slope $\frac{2}{3}$ which means that $\delta\psi$ is proportional to $N_b^{2/3}$ and to $t^{2/3}$. This behavior is shown in Fig. 7. Up to a value of $\delta\psi = 1.5°$ the measured data points fit perfectly, even for He. If the growth of the amorphous volume is now considered as $\delta\psi / N^{2/3}$ then a linear increase with $M_p^{0.75}$ is observed, as predicted by Eq. (3) (see Fig. 8 and Table I). This observed behavior is typical for our sputtering experiments but not for the bombardments. If $\log(\delta\psi)$ against $\log(N_b)$ is plotted for the bombardments then we observe an initial slope of 1. However, the observed behavior of the sputter experiments cannot be correct for a low dose, because the slope $d(\delta\psi)/dN_b$ is proportional to $N_b^{-1/3}$ and becomes infinity if N_b goes to zero. However, after a dose of $N_b \approx 10^{-3}$ Å^{-2} up to a dose N_A, as reported in Table I, the growth of the amorphous volume shows the abovementioned behavior for the sputter experiments, up to $\delta\psi \approx 1.5°$. Because after this behavior at part B the growth can be described by the model of Morehead and Crowder, it seems to be a preamorphous stage. The observed behavior proportional to $t^{2/3}$ is not explained yet, however it is interesting enough for further investigations.

IV. LOW-DOSE BEHAVIOR OF BOMBARDMENTS

In contrast to the Ne^+-ion bombardments reported previously,[2] the Ar^+ and Kr^+ results do not show a

TABLE I. A comparison between observed and calculated values for sputter experiments at 800 V and an ion flux of 115 nA/cm². E is calculated from presented experimental observations, C is calculated from theory or from given expressions in the text.

Noble gas	He	Ne	Ar	Kr	Remarks
$\delta\hat{\psi}_c$ (deg)	>6	4.14	3.43	2.94	E
d_c (Å)	>70	44.5	34.5	29.4	E
r (Å)	372.4	71.1	47.3	40.6	C
$\frac{1}{2}r\sqrt{2}$ (Å²)	263	50.3	33.4	28.7	C
A_a^B (Å²)	≈1.5	4.1	10.4	29.8	E
$\delta\hat{\psi}_B$ (deg)	≈1.4	3.01	2.72	2.18	E
d_B (Å)	≈14	30.1	27.2	21.8	E
η_d^B	≈1.1	6.2	14.2	32.5	E
E_n (eV)	512.3	711.7	737.3	748.1	C
$\bar{S}_n$ (eV/Å)	1.37	10.01	15.58	18.40	C
η_d^{35}	18.9	63.3	106	186	C
$\delta\psi/N_b^{2/3}$ (deg Å$^{4/3}$)	1.23	5.17	8.72	15.46	E
M_p (a.u.)	4	20	40	84	
$\delta\psi/(N_b^{2/3}M_p^{0.75})$ (deg Å$^{4/3}$)	0.436	0.547	0.548	0.558	E
N_A (A^{-2})	2	0.18	0.09	0.03	E

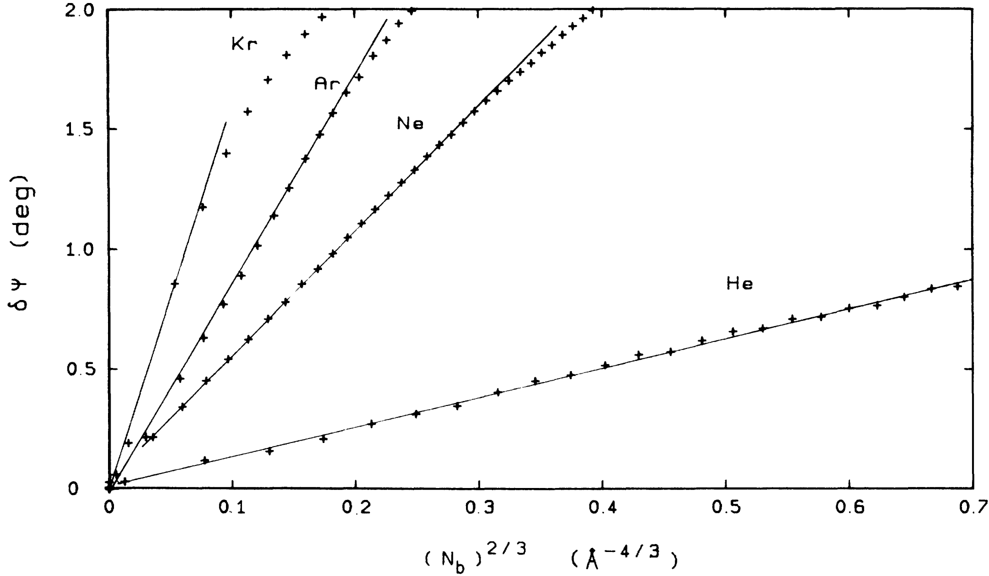

FIG. 7. The low-dose behavior of the sputter experiments as given in Fig. 5.

measurable channel behavior at the low-dose behavior. The slope along the trajectories in the $(\delta\psi,\delta\Delta)$ plane [see Fig. 1(a)] during the low-dose behavior is always directed to the same or an increasing thickness.

The initial layer thickness denoted by d_0 corresponds perfectly to calculated ranges (see Table II for a comparison of these values). Results for a 2.2-kV Ne^+-ion bombardment are also included. The characteristic area A_a can be obtained in several ways. By taking the calculated value d_0 as the layer thickness for the low-dose behavior, the value of $\tilde{\epsilon}_l$ can be obtained. Again, the values $\tilde{\epsilon}_l$ can be explained by an exponential function as has been shown previously[2] also for the pseudodielectric constant in the high-photon-energy range. Alternatively, A_a can be obtained directly from the recorded $\delta\psi$ value as pointed out in Sec. II C.

The values for A_a are collected in Table II and these will be compared with an averaged value $A_a^0=\bar{S}_n/(\bar{E}n_{\mathrm{Si}})$. The nuclear stopping power $\bar{S}_n$ is calculated[12] from the

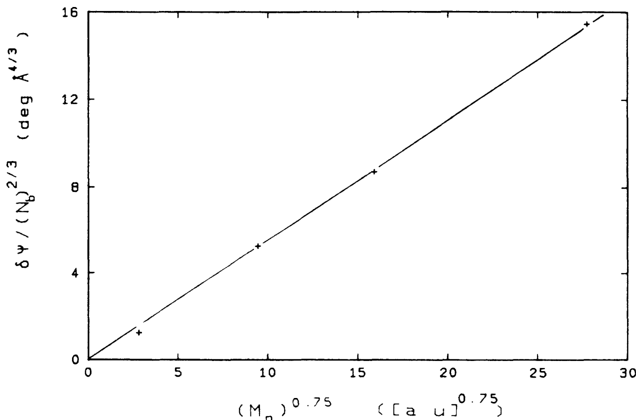

FIG. 8. The initial increment of Fig. 7 as a function of the projectile mass $M_p^{0.75}$.

energy E_n spent in nuclear collisions divided by the range r, see Table II. In Fig. 9 the experimental values of $(A_a)^{1/2}$ are plotted against the values $(\bar{S}_n)^{1/2}$. Also included are the results for the sputter experiments obtained in Sec. III at part B of Fig. 6. The results of the sputter experiments and ion bombardments at 300 K in Fig. 9 can be expressed as

$$(A_a)^{1/2}=\alpha[(S_n)^{1/2}-(S_n^{\min})^{1/2}] \tag{18}$$

with $(S_n^{\min})^{1/2}=3.05\ (\mathrm{eV/\AA})^{1/2}$ and $\alpha=5.0\ (\mathrm{\AA}^3/\mathrm{eV})^{1/2}$. At room temperature Eq. (2) predicts $(S_n^{\min})^{1/2}=3.49\ (\mathrm{eV/\AA})^{1/2}$, a value in close agreement with the observed one. However, from $\alpha=(\bar{E}n_{\mathrm{Si}})^{-1/2}$ we obtain $\bar{E}=0.8$ eV, a value much lower than predicted by Morehead and Crowder ($\bar{E}=24$ eV). Even values of $\bar{E}$ lower than 0.2 eV are reported in the literature,[6(a)] therefore we must conclude that the observed $\bar{E}$ seems realistic. The value $\bar{E}$ observed is close to the heat of melting of Si (0.8 eV in Si), suggesting that an energy-spike concept as described by Sigmund[6(b)] and Thompson *et al.*[6(c)] plays an important role.

The value η_d^0 is reported in Table II and can be compared with the number of displaced atoms η_d^{35} at 35 K as calculated from Eq. (3). For the bombardments at 2.2 keV the tendency as predicted by Eq. (3) is not observed and η_d^0 is almost constant instead of proportional to $M_p^{0.75}$.

V. HIGH-DOSE BEHAVIOR OF BOMBARDMENTS

Because the high-dose behavior of the bombardments is much more pronounced than at the sputter experiments, these will be discussed. As shown previously,[2,9] the high-dose behavior can be described by means of an increasing layer thickness:

$$d=d_0+(d_\infty-d_0)[1-\exp(-A_\infty N_b)] \tag{19}$$

TABLE II. A comparison between observed and calculated values for ion bombardments at 2.2 kV and an ion flux of 115 nA/cm^2. E is calculated from presented experimental observations. C is calculated from theory or from given expressions in the text.

Noble gas	Ne	Ar	Kr	Remarks	
d_0 (Å)	115	85	70		E
r (Å)	132.8	82.1	65.9		C
A_a (Å^2)	18	100	150	$\bar{S}_n = E_n / r$	E
E_n (eV)	1916	2014	2058	$\bar{E} = 25$ eV	C
$\bar{S}_n$ (eV/Å)	14.43	24.53	31.21		C
A_a^0 (Å^2)	11.54	19.62	24.97		C
η_d^{300}	104	425	525	$\eta_d^{300} = A_a r n_{\mathrm{Si}}$	E
η_d^0	2395	2518	2573		E
η_d^{35}	152	268	478		C
d_∞ (Å)	196	140	105		E
x_p (Å)	66.2	51.2	49.7		C
σ_x (Å)	37.0	20.7	13.1		C
$x_p + 4\sigma_x$ (Å)	214.0	134.1	102.1		C
θ_v^∞	0.13	0.10	0.08		E
N_v^∞ (Å^{-2})	1.27	0.70	0.42		E
$N_{\mathrm{ng}}^{\mathrm{bend}}$ (Å^{-2})	1.38	0.38	0.19		E
N_{ng}^∞ (Å^{-2})	1.6	0.5	0.3		E
s_{SW}	2.3	6.9	13		E
N_{sr} (Å^{-2})	0.9	0.4	0.07		E
A_∞ (Å^2)	1.7	3.3	4.5		E

while also an increasing void fraction θ_v^∞ arises. The voids do have a dielectric constant of about $1 - i0$. To get an idea of the value of d_∞ this final layer thickness is expressed in the projected range x_p and range straggling σ_x and becomes about $x_p + 4\sigma_x$.

The calculated values d_∞ and the final void fraction θ_v^∞ for 2.2-keV experiments are collected in Table II. From these values the number of collected voids $N_v^\infty = d_\infty \theta_v^\infty n_{\mathrm{Si}}$ is calculated which can be compared with the final collected amount of noble gas N_{ng}^∞, both expressed as a number per unit surface area. At first glance there seems to be an agreement between collected voids and collected noble gas.

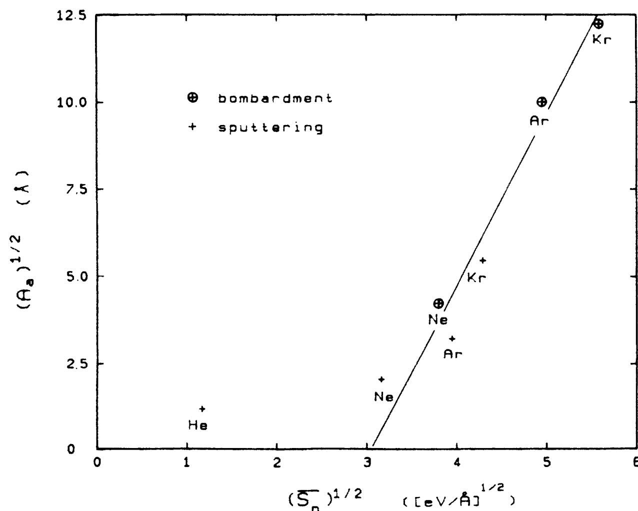

FIG. 9. The experimental values of $(A_a)^{1/2}$ compared with $(\bar{S}_n)^{1/2}$ for ion bombardment and sputter experiments. For an explanation see text.

If the observed behavior is explained by the influence of the dielectric constant of the implanted noble gas then the results can only be explained by a substitutional implantation of noble gas and at the same time a profile broadening has to arise. From the obtained desorbed doses $\hat{N}_d / N_{\mathrm{ref}}$ of the desorption experiments[3] a comparison can be made. In Fig. 10 the measured values of N_d / N_{ref} and those of $\delta\Delta$ at 700 nm are plotted against the bombardment dose N_b for the Ar^+ and Kr^+ experiments. A comparison between the final behavior of $\delta\Delta$ and the collected dose shows that $\delta\Delta$ is almost constant in the case of Kr^+ while the collected dose still increases by about 70% after point S has been reached. This is in contrast to Ar^+ where $\delta\Delta$ still changes remarkably, while the collected dose only increases by 30% after point S has been reached. Furthermore, the $\delta\Delta$ value for Ne^+ experiments already saturates at low dose even while the collected dose is proportional to a bombardment dose up to 1.5 Å^{-2} at 2.2 keV. In view of the above arguments an explanation of the high-dose behavior cannot be made only in terms of the influence of the noble gas on the

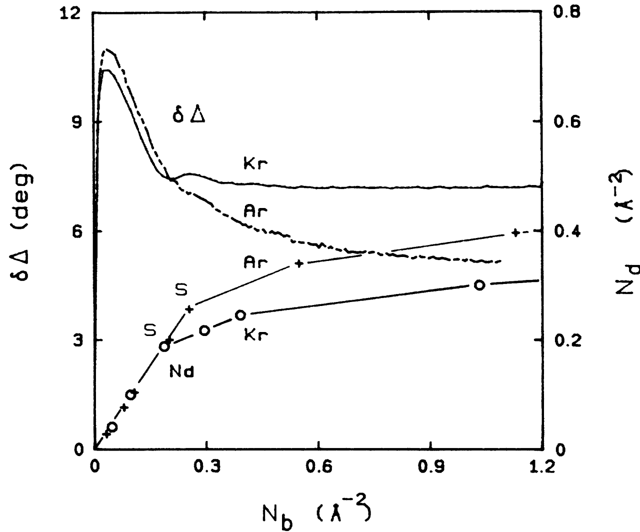

FIG. 10. A comparison between δΔ and desorbed dose N_d as a function of bombardment dose, for the 2.2-keV Ar^+- and Kr^+-ion bombardment at normal incidence ($\phi_0 = 70.25°$).

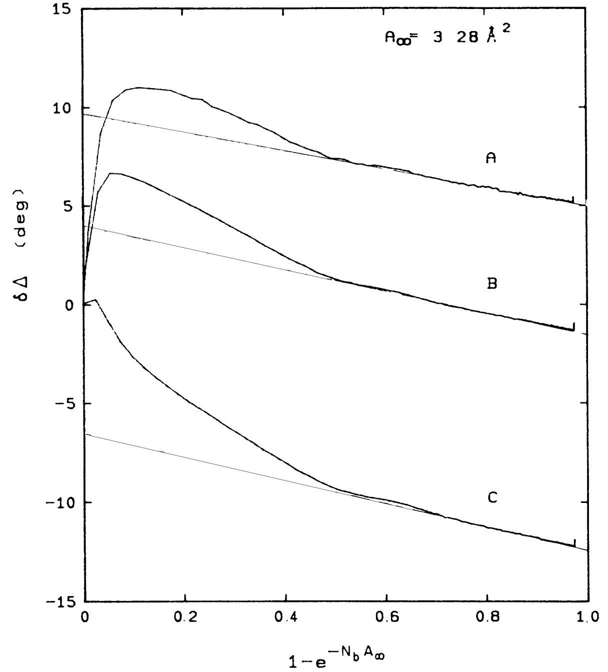

FIG. 11. The final exponential behavior of δΔ for the 2.2-keV Ar^+-ion bombardment.

dielectric constant of amorphous silicon.

If the results are explained by a dilatation or expansion of the layer due to the implantation of noble gas then θ_v^∞, as reported in Table II, gives the averaged relative dilatation. Furthermore, a profile broadening still has to be assumed while it is also not clear why the dilatation is not proportional to the collected noble gas as has been shown in detail for Ne^+.[9]

Microscopic surface roughness, arising during bombardment, can explain the above results. In Table II the observed collected noble-gas amount at the bend, N_{ng}^{bend}, is also reported. When the ion-collection model of Schulz and Wittmaack[13] is adopted, the sputter coefficient can be calculated from $s_{SW} = x_p n_{Si} / N_{ng}^{bend}$. If the surface-roughness model is adopted as given in Fig. 4(a), then after a characteristic ion dose $N_{sr} = (d_\infty - d_0) n_{Si} / (2s)$ the steady-state surface roughness can be explained (see Table II). Furthermore, with such an explanation it is not necessary to account for profile broadening at all.

As in the case of the Ne^+ experiments, the final observed behavior in δΔ and layer thickness d for the Ar^+ and Kr^+ experiments can be explained with an exponential function. This is illustrated in Fig. 11 for Ar^+. The characteristic areas A_∞ are also listed in Table II, and these values increase with increasing mass. In contrast to Ne^+, for which the high-dose behavior can be described with only one exponential function, the δΔ values of Ar^+ and Kr^+ show an exponential behavior after the noble-gas collection starts to saturate. In the case of Ar^+ the exponential function explains a layer increase of 20 Å of the rough surface layer and for Kr^+ this value is 5 Å. Before the exponential behavior the increase of the layer thickness can be described by a linear function. Therefore, the behavior of surface roughness arising during bombardment depends strongly on the chosen projectile. This is the reason why we did not report the He bombardments, because blistering effects occur even after a low dose of 1.5 $Å^{-2}$ at 2.2 keV. Those samples did not return to the original values (ψ, Δ) of c-Si after an anneal treatment.

It is still possible that all three mentioned effects, noble-gas collection, dilatation, and surface roughness, can have an influence on the observed ellipsometric behavior, but microscopic surface roughness arising during bombardment overshadows the other effects. However, it is surprising that the assumed microscopic surface roughness anneals out so well. It seems that during the amorphous-crystalline transitions even these dislocations are sweeped out. As a typical estimate on fresh samples, the $\delta\psi$ and δΔ values return after anneal within 0.1° to the starting values of the c-Si samples (except the He^+ bombardments).

VI. COMPLEMENTARY MEASUREMENTS

During the study of the high-dose behavior we observed a dilution discussed in the previous section. Of the three considered possibilities, dilatation, substitutional implanted noble gas, and surface roughness arising during bombardment, the last one seems the best possibility to explain the observed behavior by means of ellipsometry. In this section some complementary measurements are reported which support the above conclusion.

A. Dilatation: Plasmon loss peaks in the AES spectra of *c*-Si and *a*-Si

So-called plasmon loss peaks, due to collective vibrations of electrons, can be seen in an AES spectrum, for instance in the region just before the elastic peak. At normal incidence of the primary electron beam, as in our case, the excitation of surface plasmons can be neglected.[14] Therefore, only bulk plasmons will be considered.

In the case of semiconductors, the energy difference $\hbar\omega_B$ between loss peaks in the AES spectrum due to the bulk contribution is given by[15]

$$\hbar\omega_B = \hbar \left[\frac{ne^2}{m_e \epsilon_0} \right]^{1/2} , \qquad (20)$$

where n denotes the density of electrons in the covalent bonds. Assuming that a lower surface density of covalent-bond electrons is obtained after the surface layer has become amorphous, for instance due to dilatation, Eq. (20) makes it possible to observe a change in the density of electrons in the covalent bonds and therefore to determine the change of silicon atoms per unit surface in the top layer.

Figure 12 shows the plasmon loss peaks for clean *c*-Si(111) and *a*-Si recorded at an electron energy of 2 keV. The *a*-Si is obtained after sputtering with 800-eV Ar^+ ions, at a flux of 2 $\mu A/cm^2$, an angle of incidence of 45°, and a dose of 4 $Å^{-2}$. The result is surprising because no change in the plasmon energy is observed at all within an accuracy of the measurement (1% in ω_p and 2% in n). A plasmon energy of 17.6 eV is observed in both spectra. Therefore, the hypothesis of a possible extra dilatation in the surface layer due to amorphism can be rejected.

It seems reasonable that in the case of a rough surface the same plasmon loss peak will be observed as for a flat surface if locally the same surface density is present. If the transition layer of clean *c*-Si is regarded as amorphous,[16] then the result can also be understood, because the information depth of AES at a primary-beam energy of 2 keV is only 20 Å.[17]

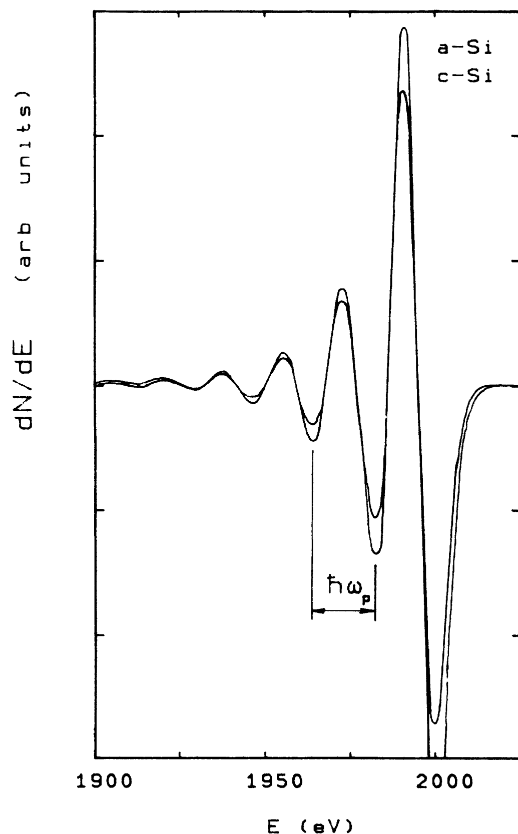

FIG. 12. The plasmon loss peaks in the AES spectra of *c*-Si and *a*-Si. The plasmon loss energy $\hbar\omega_p$ is indicated.

B. Defect creation: TEM measurements

In order to study the creation of large defects by noble-gas ion bombardment on *c*-Si, transmission electron microscopy (TEM)[11] measurements were carried out. Thin *c*-Si wafers were etched on the back to obtain a foil thickness of about 500 nm. These *c*-Si foils were bombarded with 2.2-keV Ar^+ ions at four different doses: 0.02, 0.09, 0.36, and 1.44 $Å^{-2}$.

All samples investigated with TEM show the same "pineapple-shaped" structure, which is typical for amorphous silicon samples, even at high doses. There was no evidence of large defects or bubbles. A typical estimate is that if large defects are presented, then the concentration will be lower than 10^{17} cm^{-3} and with a diameter less than 10 Å. If those defects are regarded as voids, then the volume with a diameter of 10 Å and a density of 10^{17} cm^{-3} corresponds to a void concentration of 5×10^{-5}. This void fraction is negligible compared to the observed one. Therefore, the amorphous layers of the samples are assumed to be homogeneous.

C. Surface roughness: Surface-profile measurements

The surface-profile measuring system used[18] transports a needle along the sample surface. The displacement of the needle perpendicular on the sample surface can be analyzed with suitable software and results in a graph of the perpendicular displacement against the lateral displacement in the scan direction. The radius of the needle is 0.2 μm while a needle force of 5×10^{-5} N has been used, with a scan speed of 1.1 μm/s. Therefore, only an impression of macroscopic surface roughness can be obtained. An important parameter is the depth R_A which gives the averaged vertical displacement with regard to a mean level. Alternatively, the surface roughness can be expressed as an rms value R_Q, which gives the standard deviation of the vertical depth with regard to the same mean level.

In Fig. 13 four scans are shown. In order to get an idea of the resolution of the apparatus, a measurement on a *c*-Si sample has first been carried out without a lateral displacement of the needle. In this case the measured surface roughness ($R_A = 2.0$ nm, $R_Q = 2.5$ nm) gives an impression of the background noise (see Fig. 13, needle at rest) and the horizontal lateral scale has to be converted only in this case to a time scale with the above-mentioned scan speed. The measurement carried out on *c*-Si (labeled *c*-Si) gives about the same surface roughness ($R_A = 2.1$ nm, $R_Q = 2.7$ nm) and therefore the *c*-Si sample can be regarded as macroscopically flat.

Also investigated is an *a*-Si surface obtained after a Ne^+-ion bombardment dose of 4.2 $Å^{-2}$ at 2.5 keV. In the center of the ion beam area on the sample ("Ne^+ center:" $R_A = 2.2$ nm, $R_Q = 2.8$ nm), as well as at the outside ("Ne^+ outside:" $R_A = 2.6$ nm, $R_Q = 3.4$ nm), surface roughness measurements have been carried out. The

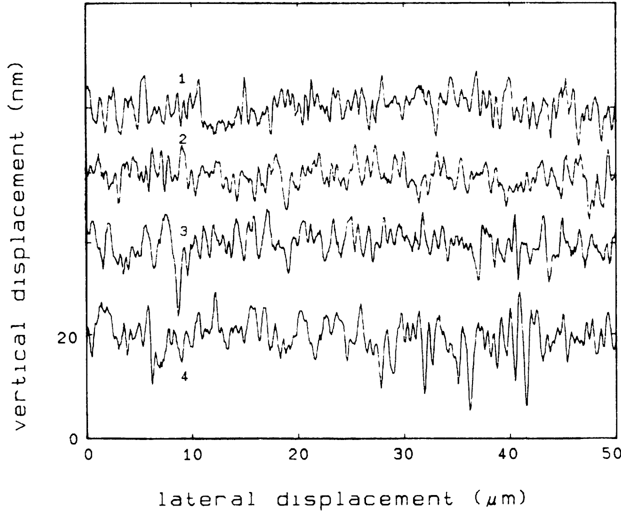

FIG. 13. Surface profile measurements. For the explanation of the labels, (1) needle at rest, (2) c-Si, (3) Ne^+ center, (4) Ne^+ outside, see text. Experimental conditions: needle force, 5×10^{-5} N; scan speed, 1.1 μm/s; filter length, 50 μm; smooth length, 0.3 μm. The vertical-displacement scale is for all experiments the same, as indicated at the left axis.

above-mentioned ion dose can be regarded as the saturation dose while for this experiment the ellipsometric measurements predict the highest microscopic surface roughness for measurements which are investigated. At least these roughness measurements indicate an increase of surface roughness due to ion bombardment, while in the Ne^+ spectra some large peaks become visible which, however, do not contribute much to the mentioned R_A and R_Q values.

From the above measurements a simple estimate for a decrease in Δ in the scope of the diffraction theory[19] for rough surfaces is possible. If the correlation length T is established as the averaged distance between the peaks in the spectra of Ne^+ as 0.5 μm, then a parameter $\tan(\beta_0)=R_Q(2/T)^{1/2}<10^{-2}$ (Ref. 19, p. 114) has to explain the decrease in Δ. From this value a decrease in Δ of only 0.1° will appear (Ref. 19, p. 98) at $\lambda=546.1$ nm due to macroscopic surface roughness, which is negligible compared to the observed large decrease of the order of 15°.

For a microscopic indication of surface roughness a more direct approach is to use scanning tunneling microscopy (STM) as done by Feenstra and Oehrlein.[20] They claim a 0.5 Å vertical and 10 Å lateral resolution with STM for topographical images of silicon samples. The observed rms surface roughness of their samples before bombardment shows an averaged value of 1.8±0.4 Å. After an Ar^+-ion bombardment at 700 V and an ion dose of 100 $Å^{-2}$ with a broad-beam ion source, they observe a surface covered with small hillocks, typically 50 Å in diameter and about 10 Å high. The rms value is about 3.9 Å.

This situation can be compared with the Ne^+ bombardments as reported previously by us,[2] which gives a similar value for the ellipsometric microscopic surface roughness of Ne^+ at about 500 V.

VII. SELF-ANNEAL BEHAVIOR

In order to study the self-anneal behavior as a function of the substrate temperature, c-Si(111) surfaces are sputtered with Ar^+ at a low ion dose with an acceleration voltage of 800 V, an angle of incidence of 45°, and a flux of 115 nA/cm^2. Under these conditions the value of $\delta\psi$ is directly related to the volume of amorphous silicon and broken bonds, as shown in Sec. II C. Furthermore, at low ion dose, only the amorphization plays a role.

After the low ion dose at different substrate temperatures the self-anneal behavior is ellipsometrically recorded. A typical example is shown in Fig. 14(a). The changes of $\delta\psi$ after termination of the sputter process show a fast and a slow change. If the curve describing the slow change BC is extrapolated to A, the change $\delta\psi_f$ can be described with an exponential function [see Fig. 14(b)]

$$\delta\psi_f=\delta\hat{\psi}_f e^{-t/\tau_f} . \tag{21}$$

The time constants τ_f are determined as a function of the substrate temperature in the range 550–150 K. At high temperatures the value $\delta\hat{\psi}_f$ is so small that the relaxation

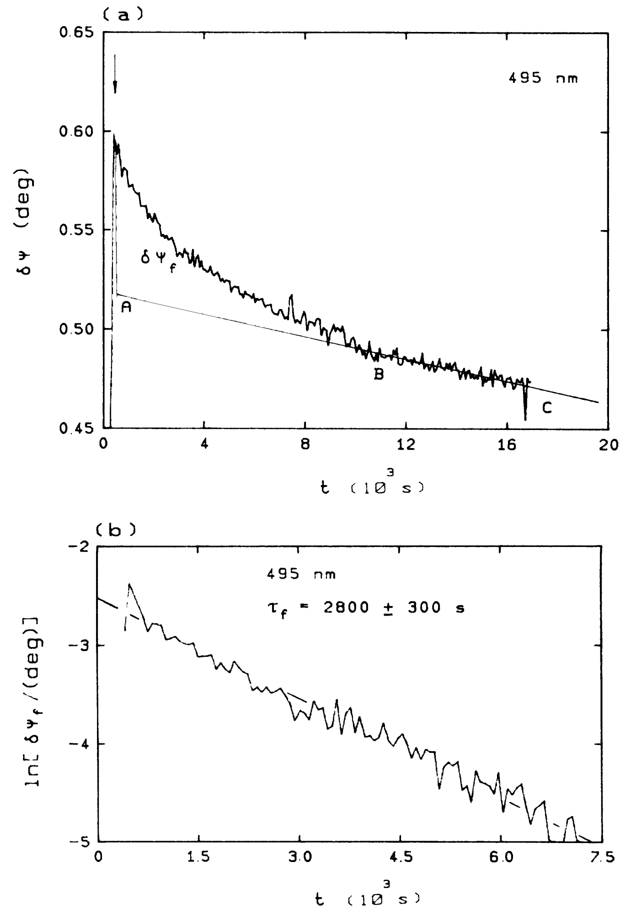

FIG. 14. (a) A typical example of the self-anneal behavior after a low ion dose. The arrow indicates the termination of the sputter experiment of Ar^+ at 800 V, at a flux of 115 nA/cm^2 and at an angle of incidence of 45° ($\phi_0=70.25°$). (b) The fast change $\delta\psi_f$ after termination of the sputter experiment at point A as indicated in (a).

time τ_f cannot be determined at all. At low temperatures the "fast" change becomes a slow one and then the value of τ_f has been determined from the start direction

$$\frac{1}{\delta\hat{\psi}_f}\frac{d(\delta\psi_f)}{dt}\bigg|_{t=0}=-\frac{1}{\tau_f}\,. \tag{22}$$

Therefore the error in τ_f becomes higher at a lower temperature, because the value of $\delta\hat{\psi}_f$ is not precisely determined.

In Fig. 15 the values of the logarithm of τ_f are plotted against the reciprocal temperature $1/T$. It turns out that τ_f can be described as

$$\tau_f=\tau_0 e^{E_a/kT} \tag{23}$$

with $\tau_0=160$ s and an activation energy $E_a=64\pm4$ meV. The value of E_a can be understood within the scope of the model of Morehead and Crowder. In this model the radius of the area A_a^0 relaxes in short times as $\delta R \sim 2(Dt)^{1/2} \sim e^{-E/2kT}$, while in fact these authors determine a fitting parameter $E_a=E/2=60$ meV from available literature data.[5] So it seems that the self-anneal behavior is governed by the diffusion of vacancies with the same activation energy as that which describes the relaxation of area A_a^0 to A_a.

The order of time constant τ_0 observed is not clear yet. A possible explanation can be that the vacancies which diffuse during the self-anneal behavior have to travel a large distance before they anneal out completely. Furthermore, if the above experiments are repeated after a high dose, about the same time constants τ_f as a function of the temperature have been observed. A typical example is given in Fig. 16. Therefore, it can be concluded that the self-anneal behavior reflects the diffusion mechanism of vacancies. At the same time covalent bonds are restored, because the band gap E_{g0} increases as shown by previous measurements.[2]

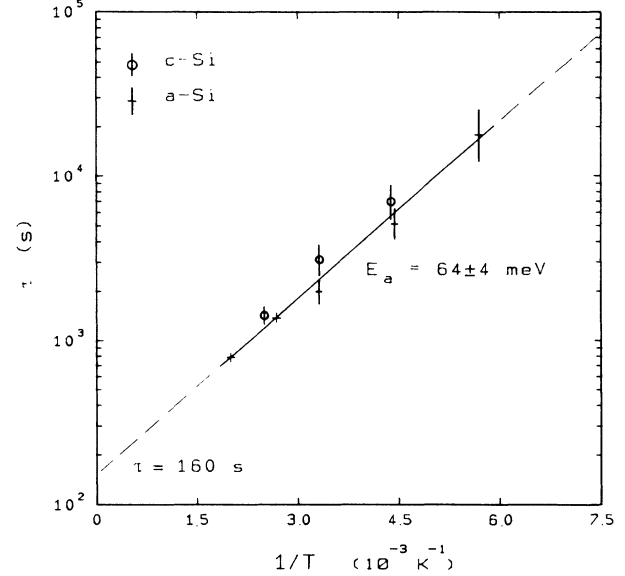

FIG. 15. The time constant τ_f as a function of the reciprocal substrate temperature. Indicated are results for low-dose experiments (c-Si) and for high-dose experiments (a-Si), as illustrated in Figs. 14 and 16, respectively.

VIII. CONCLUSIONS

At the low-dose bombardment on clean c-Si samples the fraction θ_a of amorphous silicon in the scope of a three-phase system can be expressed as

$$\theta_a=1-\exp(-A_a N_b)$$

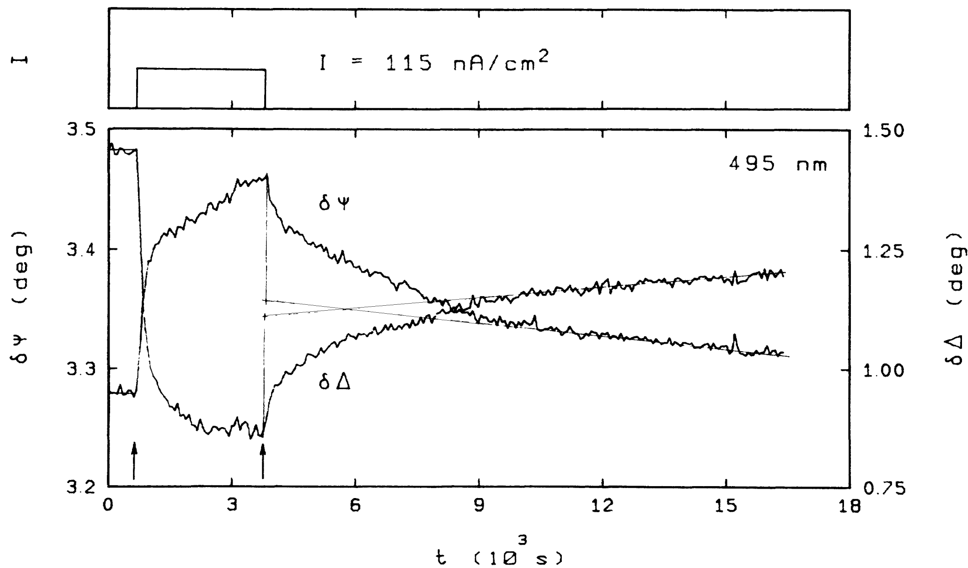

FIG. 16. A typical example after a high-dose (4 Å^{-2}) sputter experiment of the self-anneal behavior after termination of the sputter experiment for the second time. The first arrow is the start of the stepwise-shaped ion current while the sample has been self-annealed for 1 hr after a high dose. The second arrow indicates the second termination of the sputtering process.

while a layer thickness d_0 becomes amorphous. The value d_0 corresponds with a calculated ion range r (Ref. 12) as predicted by the ion-range theory. The characteristic area A_a^0 can be explained by the model of Morehead and Crowder.[5]

There are two interesting ellipsometric situations where the amorphization can be studied without a precise knowledge of the dielectric constants.

If the intensity penetration depth of light is much lower than the range r, direct observation of θ_a as a function of dose N_b is possible because the sample seems to change to an infinite thickness due to ion bombardment. In such a case the pseudodielectric constant, which can be calculated directly, is a very good estimate for the real one and reflects the amorphization.[2]

Another interesting situation discussed here is the case of the intensity penetration depth of light being much larger than the range r and a direct observation of the number of initial displaced atoms η_d being possible. By measuring $\delta\psi$ ($\delta\psi < 2.5°$ at 495 nm) the value η_d can be obtained from $\delta\psi/\beta$, where β denotes a wavelength-dependent constant. This is an ideal situation for studying the initial behavior of the amorphization. It turns out for sputtering experiments, for instance, that before the final behavior $\theta_a = 1 - e^{A_a N_b}$ is observed, a preamorphous stage first arises, described by

$$\eta_d \simeq N_b^{2/3} M_p^{0.75} \quad \text{for } N_b > 10^{-3} \text{ Å}^{-2} .$$

In other cases the dielectric constants $\tilde{\epsilon}_c$ and $\tilde{\epsilon}_a$ have to be known. The model as proposed by Davis and Mott[21] can be used successfully to describe the value of ϵ_{2a} in the low-photon-energy range.[2] By using a linear regression technique layer thicknesses can be obtained.[2,9]

At the high-dose behavior a dilution arises. A direct observation is possible at a layer thickness higher than the intensity penetration depth.[2] Also a linear relation between the $\delta\Delta$ indicates a dilution.

The final observed behavior at the bombardments with respect to the layer thicknesses for Ne^+ at $N_b > 0.03$ Å^{-2} is the most simple one, with

$$d_\infty = d_0 + (d_\infty - d_0)(1 - e^{-A_\infty N_b})$$

and where the sputter coefficient is given by

$$s = \tfrac{1}{2} A_\infty (d_\infty - d_0) n_{\text{Si}} .$$

Also the Ar^+ and Kr^+ bombardments finally show this exponential behavior, while a linear increase of d is first observed as a function of N_b.[9]

By making use of a four-phase system instead of a three-phase system it can be shown that the dilution is present at the front of the sample because such an assumption remarkably reduces the standard deviation in the calculation with linear regression.[9] Of all possible effects which can explain a dilution, *in situ* ellipsometry observes only the dilution. Therefore some complementary measurements are carried out. For several reasons the best explanation of the experimental results for the high-dose behavior seems to be microscopic surface roughness arising during bombardment. First, the increase from a layer thickness r after the low-dose behavior up to a layer thickness d_∞ at the high-dose behavior in the steady state, can be explained by a sputter coefficient which at the same time explains the observed collection of noble gas. Secondly, a profile broadening from a value r up to $d_\infty \gg r$ is difficult to explain by the theory of ion ranges in the solid. However, if microscopic surface roughness arises then the final layer thickness described by a three-phase system becomes $(d_\infty - r) + r$, because the deepest pits also act as starting points for ion trajectories with range r. Thirdly, the complementary measurements do not support the hypothesis of dilatation or substitutionally implanted noble gas clusters to defects, but indicate surface roughness.

At the termination of ion bombardment or sputter experiments the ellipsometric values $\delta\psi$ and $\delta\Delta$ still vary. This can be explained by a partial recovery to a more stable phase while the damaged layer thickness remains the same.[3] The optical band gap E_{g0} increases after termination of implantation (with about 0.04 eV at Ne^+-ion bombardments), which can be explained in the scope of the model of Davis and Mott by a partial restoration of covalent bonds.

It turns out from the stepwise-shaped sputter experiments that the self-anneal behavior as a function of temperature can be described by the same activation energy E_a as the one which explains the shrinking of area A_a^0 to A_a in the model of Morehead and Crowder during bombardment or sputtering. The observed time constants, which describe the relaxation from the steady-state values to a more stable phase after termination of the bombardment, can also explain the observed behavior at a lower ion flux.[1] This indicates that during bombardment a recovery occurs in such way that at a low flux the layer is not built up completely. The previously mentioned effects of the high-dose and self-anneal behaviors explain why so many different dielectric constants of amorphous silicon are reported in the literature.

ACKNOWLEDGMENTS

The TEM measurements were carried out at the Philips Research Laboratories at Eindhoven. I would like to thank Dr. M. P. A. Viegers for the preparation of the thin *c*-Si foils and the TEM measurements of the samples. The measurements with the surface profiler have also been carried out at the Philips Research Laboratories at Eindhoven and I would like to express my gratitude to J. van der Linden and Dr. P. E. Wierenga for their measurements. This work is part of the research program of the "Stichting voor Fundamenteel Onderzoek der Materie" (Foundation for Fundamental Research of Matter) and was made possibly by financial support from the "Nederlandse Organisatie voor Wetenschappelijk Onderzoek" (Netherlands Organization for the Advancement of Pure Research).

[1]A. H. M. Holtslag, U. C. Slager, and A. van Silfhout, Surf. Sci. **152/153**, 1079 (1985).

[2]A. H. M. Holtslag and A. van Silfhout, Nucl. Instrum. Methods Phys. Res. B **19/20**, 585 (1987).

[3]A. H. M. Holtslag and A. van Silfhout, Surf. Sci. **187**, 36 (1987).

[4]G. H. Kinchin and R. S. Pease, Rep. Prog. Phys. **18**, 1 (1955).

[5]F. F. Morehead and B. L. Crowder, Radiat. Eff. **6**, 27 (1979).

[6](a) N. A. G. Ahmed, C. E. Christodoulides, and G. Carter, Radiat. Eff. **38**, 221 (1978); (b) P. Sigmund, Appl. Phys. Lett. **25**, 169 (1974); (c) D. A. Thompson, R. S. Walker, and J. A. Davies, Radiat. Eff. **32**, 135 (1977).

[7]R. M. A. Azzam and N. M. Bashara, *Ellipsometry and Polarized Light* (North-Holland, Amsterdam, 1977).

[8]D. E. Aspnes, Am. J. Phys. **50**, 704 (1982).

[9]A. H. M. Holtslag, thesis, Twente University of Technology, 1986.

[10]B. L. Schram, thesis, University of Amsterdam, 1966.

[11]J. F. Gibbons, Proc. IEEE **60**, 1062 (1972).

[12]J. F. Ziegler, J. P. Biersack, and U. Littmark, *The Stopping and Range of Ions in Solids* (Pergamon, New York, 1985), Vol. 1.

[13]F. Schutz and K. Wittmaack, Radiat. Eff. **29**, 31 (1976).

[14]H. Raether, in *Excitation of Plasmons and Interband Transitions by Electrons,* Vol. 88 of *Springer Tracts in Modern Physics* (Springer-Verlag, Berlin, 1980), p. 116.

[15]C. Kittel, *Introduction to Solid State Physics* (Wiley, New York, 1976), p. 293.

[16]F. Meyer, E. E. De Kluizenaar, and G. A. Bootsma, Surf. Sci. **27**, 88 (1971).

[17]A. W. Czanderna, *Methods of Surface Analysis* (Elsevier Scientific, Amsterdam, 1975), p. 108.

[18]P. E. Wierenga and A. J. J. Franken, Philips Tech. Rev. **42**, 85 (1985).

[19]I. Ohlidal, F. Lukes, and K. Navrátil, Surf. Sci. **45**, 91 (1974).

[20]R. M. Feenstra and G. S. Oehrlein, Appl. Phys. Lett. **47**, 97 (1985).

[21]E. A. Davis and N. F. Mott, Philos. Mag. **22**, 903 (1970).